

CFO-Robust Detection for 5G PRACH under Fading Channels: Analytical Modeling and Performance Evaluation

Daniel Alarcón-Martín, Mari Carmen Aguayo-Torres, Francisco J. Martín-Vega, and Gerardo Gómez

Abstract—The Physical Random Access Channel (PRACH) is essential for initial access and synchronization in both 5G and future 6G networks; however, its detection is highly sensitive to impairments such as high user density, large carrier frequency offset (CFO), and fast fading. Although prior studies have examined PRACH detection, they are often restricted to specific scenarios or lack a comprehensive analytical characterization of performance. We introduce a unified analytical framework that characterizes the statistical distribution of the received power delay profile (PDP) under flat Rayleigh fading and supports both coherent combining (CC) and power combining (PC) repetition strategies. For each strategy, we derive optimal threshold expressions and closed-form detection probabilities. Furthermore, we analyze two key cases depending on the coherence time: identical and independent channel realizations per repetition. Secondly, we exploit the correlation induced by CFO across cyclic shifts to design a novel low-complexity detector that exploits PDP dependencies. Numerical results indicate that PC outperforms CC when repetitions experience independent channels, while CC can be preferable under identical realizations in limited settings. On the other hand, the proposed CFO-aware detector delivers improved robustness under severe CFO conditions.

Index Terms—PRACH, Random access, 5G, Detector.

I. INTRODUCTION

A. Motivation and scope

THE proliferation of 5G networks marks a new era of connectivity characterized by high data rates, ultra-low latency, massive device connectivity, and enhanced reliability. A key aspect of this advancement lies in Physical Random Access Channel (PRACH) [1], which plays a pivotal role in establishing communication between the user equipment (UE) and the network. PRACH serves as the initial handshake in the access procedure, facilitating uplink (UL) synchronization and initial beam selection for data transmission [2]. However, due to the increasing variety of use cases, traditional PRACH preamble detection mechanisms face significant challenges. The rising complexity of 5G scenarios introduces issues such as high user density, larger carrier frequency offset (CFO), and fast fading. To address these challenges, the 5G standard has considerably extended PRACH, introducing a diverse set of

preamble formats with increased preamble repetitions, diverse subcarrier spacing (SCS) and shorter preamble length. This leads to the configuration of a larger number of roots per Next Generation Node B (gNB) to reduce collision rates, increasing interference between roots, and resulting in inefficient use of radio resources. These issues are expected to persist or intensify in future 6G systems, especially when considering the integration of non-terrestrial networks (NTN), spatial multiplexing, and grant-free random access (RA).

B. Related work

Several works in the literature address these issues by analyzing PRACH preamble detection in scenarios such as 5G cellular networks [3] [4] [5]. These works consider detectors that compare the power delay profile (PDP) of the received preambles with a unique threshold whose value is fixed and must satisfy a target false alarm probability. Peaks in the PDP with a higher amplitude than this threshold are used to estimate the round-trip propagation delay that is used for timing advance [6]. Therefore, designing a detector requires a thorough statistical analysis of the received preamble. Some of these works make simplifying assumptions about the system model, such as a single receiver antenna, a single-user transmission, or a single-root configured base station. Meanwhile, other works do not analyze the statistical performance and properties of their models.

While these assumptions are valid for LTE scenarios, they do not hold for the more robust and complex 5G scenarios. Indeed, as demonstrated in this work, the CFO experienced by the signal must be carefully addressed to maximize preamble detection while fulfilling a given target false alarm probability. Modeling this behavior is very challenging, as it depends on the specific frequency offset of each user, the number of users transmitting in the same PRACH occasion, and the number of roots assigned to the gNB.

The analysis of CFO in a multi-user scenario, where the preambles are non-orthogonal, is substantially more complex than the previously analyzed cases, e.g., considering either a single-user with CFO or a multi-user case with a flat fading channel without CFO. In particular: i) in the presence of CFO, the statistics of the PDP depend on the user's Doppler shift; therefore, the performance depends on the type of scenario; ii) each preamble in the same PRACH occasion interferes with the others; iii) unlike a flat channel, the interference between different roots is not constant.

This work has been funded by MCIN/AEI/10.13039/501100011033 (Spain), by the European Fund for Regional Development (FEDER) 'A way of making Europe', and the University of Málaga through grants PID2020-118139RB-I00 and RYC2021-034620-I.

The authors are with the Communications and Signal Processing Lab, Telecommunication Research Institute (TELMA), Universidad de Málaga, E.T.S. Ingeniería de Telecomunicación, Bulevar Louis Pasteur 35, 29010 Málaga (Spain). (e-mail: {dalarcon,aguayo}@ic.uma.es)

TABLE I
LIST OF RELATED WORKS.

Ref.	Detection anal.	False alarm anal.	Channel model	Multi-user	Multi-root	Multi-antenna	Multi-repetitions	Year
[7]	Yes*	Yes*	Multipath with CFO	No	No	No	No	2018
[8]	No	No	Multipath with CFO	Yes	No	No	No	2015
[9]	Yes*	Yes*	Multipath	No	No	Yes	No	2013
[10]	No	No	Multipath with CFO	No	No	No	No	2013
[11]	Yes	No	Flat channel	Yes	Yes	Yes	No	2019
[12]	Yes*	Yes	Flat channel	Yes	Yes	No	No	2017
[13]	No	No	Flat channel with CFO	No	No	Yes	Yes	2019
[14]	Yes	Yes	Flat channel	Yes	No	No	No	2016
[15]	No	No	Multipath with CFO	Yes	No	Yes	Yes	2023
Proposed	Yes	Yes	Flat channel with CFO	Yes	Yes	Yes	Yes	-

Note: the Yes* tag means that the analysis is not done analytically.

Despite its relevance, analysis of PRACH detectors in the presence of CFO is scarce. Most existing works avoid the need to calculate the statistics of their designed detectors, either because they consider a PRACH configuration that is minimally affected by CFO, or because their detection algorithms are complex. Moreover, most of the work has been done for LTE, while new aspects of 5G remain unexplored. A list of related works is given in Table I. For example, in [11], asymptotic probability-density-function expressions are derived to detect Gaussian and Zadoff–Chu (ZC) sequences over a Rayleigh channel accounting for multiple roots, users, and antennas; although they use a non-standard ZC length and omit any CFO. [7] introduces a CFO-aware framework using a generalized likelihood-ratio test under unknown multipath, but does not analytically derive optimal detector parameters and ignores the effects of multiple receive antennas, simultaneous users, or multiple roots. [10] formulate a transform-domain model that incorporates user channel impulse responses, timing offsets, CFO, and propose a multi-step reconstruction algorithm that suppresses inter-user interference, although they do not derive closed-form expressions for success and false alarm probabilities. [15] investigate coherent combining (CC), performed on the individual in-phase and quadrature components, and power combining (PC), i.e. on their squared combination, in the presence of CFO with multi-antenna and multi-users but only via simulations, resulting in a lack of a theoretical framework, which hinders practical applicability in 5G. Therefore, as seen in Table I, there is a notable gap related to analysis of PRACH detection in multi-user scenarios with CFO, which is of paramount importance in practical settings.

C. Main contributions

To our knowledge, theoretical analysis of success detection and false alarm probabilities in the presence of CFO has not yet been derived for a particular detector in the case of multiple antennas, multiple users, and multiple roots despite its relevance for robust and efficient 5G cellular planning, which motivated us to address this research gap. The main contributions of this work are:

- 1) We present a mathematical framework to obtain the PDP statistics, considering the Rayleigh channel case and its extension including CFO for a multi-antenna, multi-user, multi-root scenario.

- 2) We analyze different types of signal combining for the preamble reception, showing results for different PRACH formats.
- 3) We derive closed-form expressions for success detection and false alarm probabilities of a novel statistically-informed detector that takes CFO into account.
- 4) Finally, we discuss and illustrate the usefulness of the expressions by analyzing success and false alarm probabilities versus those of a conventional detector.

The designed detector also aims to improve the inefficient use of radio resources. As mentioned above, due to CFO and the need for more roots, interference between them increases, and consequently, false alarms and the radio resources allocated to respond to them also increase. This effect can be mitigated by using formats with larger SCS, but then more bandwidth will be used for PRACH transmission, and the effects of multiple roots will still persist. Our CFO-based detector aims at reducing these effects avoiding the need to increase SCS and thus improving network efficiency.

The rest of the work is structured as follows. In Section II, an overview of PRACH is provided, explaining its parameters and its role within the RA procedure. In Section III, the system model is described, detailing the transmission and reception of PRACH. In Section IV, the derivation and analysis of PDP statistics for different signal combiners are performed. The optimal threshold for the case of a flat channel without CFO is presented in Section V. In Section VI, a novel detector developed in the presence of CFO is explained. Numerical results are presented in Section VII. Finally, conclusions are drawn in Section VIII.

II. PRACH OVERVIEW

In 5G New Radio (NR), the UE initiate communication with the network by transmitting a randomly selected preamble during specific time-frequency resources known as PRACH occasions. These occasions are defined and broadcasted by the gNB and are crucial to coordinating contention-based access in a scalable and efficient manner. Each PRACH occasion is characterized by several configuration parameters [1]:

- The PRACH *ConfigurationIndex* parameter determines the time and frequency resources allocated within a radio frame.
- The SCS, defining the numerology for PRACH transmission, supports a wide range such as 1.25 kHz, 5 kHz

or from 15 kHz to 240 kHz, to accommodate diverse deployment scenarios.

- The PRACH *Format* dictates the sequence length, cyclic prefix (CP), sequence repetitions, and time-domain guards, enabling flexible adaptation to requirements such as coverage or latency.
- The PRACH *SequenceIndex* parameter specifies which root sequence is used as the basis for all preambles.

PRACH preambles are based on Zadoff–Chu (ZC) sequences, which exhibit excellent autocorrelation and low cross-correlation properties. The network determines a root and applies cyclic shifts (CSs) to generate multiple preambles while preserving the zero-correlation zone. If additional preambles are required, multiple roots can be configured, allowing expansion in the code-domain. Combined with multiplexing in the time and frequency domains through separate PRACH occasions, this approach allows massive user access with minimal contention.

Power control is performed based on the estimated path-loss and the target receive power parameter P_0 configured by the cell [16]. Then, the gNB detects preambles by computing cross-correlation and derives a random access radio network temporary identifier (RA-RNTI) that identifies the PRACH occasion. It transmits the Random Access Response (RAR), which includes a timing advance command, an UL grant for further communication, and possibly initiates contention resolution. The UE monitors for a RAR from the gNB to respond with an UL transmission named *message 3* (Msg3).

In cases of preamble collision, where multiple UEs select the same resources, the gNB responds with a common RAR. Only one UE's subsequent message may be successfully decoded, and contention is resolved through a dedicated message (Msg4) carrying the cell radio network temporary identifier (C-RNTI) of the successful UE. While undetected transmissions result in access retries, false alarms waste resources; thus, 5G NR specifications strictly regulate detection and false alarm probabilities to maintain access efficiency.

A. Notation

We consider sequences of finite length ℓ , $\{x[n]\}_{n=0:\ell-1}$. In vector form, $\mathbf{x} = \{x[n]; n = 0, 1, \dots, \ell - 1\}$. Discrete Fourier transform (DFT) of the finite length discrete sequence is $\mathbf{X} = \text{DFT}\{\mathbf{x}\} = \{X[\nu]; \nu = 0, 1, \dots, \ell - 1\}$ with $X[\nu] = \sum_{n=0}^{\ell-1} x[n]e^{-j\frac{2\pi n\nu}{\ell}}$. The periodic cross-correlation between two finite-length discrete sequences, \mathbf{x} and \mathbf{y} of the same length can be expressed as $\mathbf{c} = \mathbf{x} \star \mathbf{y}$ and its term evaluated as: $c[k] = \frac{1}{\ell} \sum_{n=0}^{\ell-1} x[n]y^*[(n-k)_\ell]$, where \star means the circular cross-correlation operation, $(\cdot)^*$ denotes the complex conjugate, and $(\cdot)_\ell$ denotes the modulus- ℓ operation. It can also be evaluated in the frequency domain using the inverse discrete Fourier transform (iDFT) as $\mathbf{c} = \mathbf{x} \star \mathbf{y} = \text{iDFT}\{\mathbf{X} \odot \mathbf{Y}^*\}$, with \odot meaning point-to-point multiplication.

Notation relative to random variables and vectors, as well as some distributions useful along this text, can be found in the Appendix.

B. Zadoff-Chu sequences

PRACH preambles in 5G are based on ZC sequences, a class of polyphase sequences defined as [1]:

$$\mathbf{x}_u = \{x_u[n] = e^{-\frac{j\pi un(n+1)}{\ell}}; n = 0, 1, \dots, \ell - 1\}, \quad (1)$$

where ℓ is the sequence length and u is the root of the sequence, relatively prime to ℓ .

A set of random access sequences with the same root can be obtained by cyclically shifting the original ZC sequence for a given u root, and CS, κ_v , as follows [1]:

$$\mathbf{x}_{u,v} = \left\{ x_{u,v}[n] \triangleq x_u[(n + \kappa_v)_\ell]; n = 0, 1, \dots, \ell - 1 \right\}, \quad (2)$$

where CS $\kappa_v \in \mathcal{K}$ is one of the CSs available in the set that contains the permitted CSs relative to the original ZC sequence in eq. (1) of root u . The set of valid u -roots is given in [[17] Tables 6.3.3.1-3 to 6.3.3.1-4B], and are chosen so that the interference between them is minimal.

C. ZC sequences in 5G NR

In principle there are $\ell - 1$ different cyclic shifts. However, a limited set \mathcal{K} is employed in 5G [1], defined with a certain CS granularity, $n^{(\text{CS})}$:

$$\mathcal{K} = \left\{ \kappa_v = vn^{(\text{CS})}; v = 0, 1, \dots, \left\lfloor \frac{\ell}{n^{(\text{CS})}} \right\rfloor - 1 \right\}. \quad (3)$$

Consequently, there are $\lfloor \frac{\ell}{n^{(\text{CS})}} \rfloor$ different CSs per root. Thus, if a sequence is delayed, a guard time is kept around those employed CSs at the expense of limiting the number of different sequences for a certain root. This guard is named zero-correlation zone, its width is $n^{(\text{CS})}$, and it is determined by a radio resource control (RRC) message containing the *zeroCorrelationZoneConfig* parameter [1]. It depends on the range of the area to be served, as it tries to mitigate imbalances such as timing offsets and channel delay spread. In contrast, this reduces the number of preambles per root.

D. Cross-correlation between ZC sequences

We define the cross-correlation between two cyclic shifted ZC sequences as:

$$\mathbf{c}_{u_1, v_1, u_2, v_2} = \mathbf{x}_{u_1, v_1} \star \mathbf{x}_{u_2, v_2}. \quad (4)$$

For a given root u_0 , the ZC sequence possesses an ideal periodic autocorrelation property: the sequences obtained from cyclically shifting the same ZC sequence are orthogonal, i.e., they exhibit zero cross-correlation and perfect autocorrelation [2, Ch. 3]:

$$c_{u_0, v_1, u_0, v_2}[k] = \delta[(k - (\ell + \kappa_{v_2} - \kappa_{v_1}))_\ell], k = 0, \dots, \ell - 1, \quad (5)$$

where $\delta[n]$ is the Kronecker delta, which is 1 for $n = 0$ and 0 otherwise.

For different root values, the cross-correlation is not zero, but is instead equal to a constant value [2, Ch. 3]:

$$c_{u_1, v_1, u_2, v_2}[k] = \frac{1}{\sqrt{\ell}}, k = 0, \dots, \ell - 1, u_1 \neq u_2. \quad (6)$$

E. Cross-correlation between frequency-shifted ZC sequences

A shift in frequency ϵ produces a modulation, i.e., it results in a new sequence given by:

$$\mathbf{x}_{u,v}^\epsilon = \left\{ x_{u,v}[n] e^{\frac{j2\pi\epsilon n}{\ell}}; n = 0, 1, \dots, \ell - 1 \right\}. \quad (7)$$

We define the cross-correlation between one shifted sequence and another reference sequence as:

$$\mathbf{c}_{u_1, v_1, u_2, v_2}^{\epsilon_1} = \mathbf{x}_{u_1, v_1}^{\epsilon_1} \star \mathbf{x}_{u_2, v_2}. \quad (8)$$

Then, the cross-correlation between the sequence $\mathbf{x}_{u_g, v_g}^{\epsilon_g}$ and a non-shifted reference sequence $\mathbf{x}_{u_0, 0}$ can be evaluated as:

$$\begin{aligned} \mathbf{c}_{u_g, v_g, u_0, 0}^{\epsilon_g}[k] &= \frac{1}{\ell} \sum_{n=0}^{\ell-1} x_{u_g, v_g}[n] e^{\frac{j2\pi n \epsilon_g}{\ell}} x_{u_0, 0}^*[n-k]_\ell = \\ &= \frac{1}{\ell} e^{\frac{-\pi u_g v_g (v_g + 1) + \pi u_0 k (k-1)}{\ell}} G(u_0 - u_g, \alpha(k) - \epsilon_g), \end{aligned} \quad (9)$$

where $k = 0, \dots, \ell - 1$; $\alpha(k) = u_g v_g + u_0 k + \frac{1}{2}(u_g + u_0)$; and $G(a, b)$ is a quadratic Gauss sum [18], defined as:

$$G(a, b) = \sum_{n=0}^{\ell-1} e^{\frac{j\pi a n^2}{\ell} - \frac{j2\pi b n}{\ell}}. \quad (10)$$

III. SYSTEM MODEL

We consider a single-cell network in which the gNB configures $n^{(\text{root})}$ root sequences, collected in the set \mathcal{R} , to generate PRACH preambles. In a given PRACH occasion, $n^{(\text{dev})}$ devices attempt RA for UL transmissions. Let $n_{u_p}^{(\text{dev})}$ denote the number of devices selecting root index $u_p \in \mathcal{R}$, for $p = 0, 1, \dots, n^{(\text{root})} - 1$, to generate their preambles. We denote \mathcal{D} the set of all active devices transmitting at the considered PRACH occasion. The total number of devices is thus $n^{(\text{dev})} = \sum_{p=0}^{n^{(\text{root})}-1} n_{u_p}^{(\text{dev})}$. Without loss of generality, we consider u_0 as the reference root, and $\bar{\mathcal{D}}_{u_0}$ is the subset of \mathcal{D} formed by $n_{u_0}^{(\text{inter})} = n^{(\text{dev})} - n_{u_0}^{(\text{dev})}$ active devices that are not transmitting with u_0 , but with a different root.

A. PRACH transmitter

A PRACH transmitter follows the next steps (see Fig. 1):

- 1) The g -th device randomly selects a cyclic shift from one of the configured roots $u_{(g)}$. Then, it generates a ZC sequence, applying the selected CS κ_{v_g} to derive the actual sequence $\mathbf{x}_{u_{(g)}, v_g}$.
- 2) Obtain its frequency domain representation $X_{u_{(g)}, v_g}$ as its DFT.
- 3) Allocate the sequence at the ℓ subcarriers appropriate for the corresponding PRACH occasion.
- 4) Perform single carrier modulation using an inverse DFT. Transmit the result $n^{(\text{rep})} \geq 1$ times, as described by the selected format. A CP is appended after the last repetition; intermediate CPs are not required, as the previous repetition provides the required guard interval.
- 5) Apply the open-loop power control [16] by adjusting the transmitted power such that the Preamble Received Target Power is achieved at the gNB.

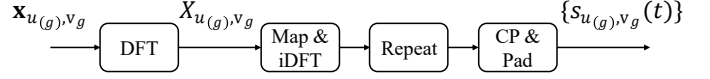


Fig. 1. The g -th device PRACH transmitter.

The transmitted sequence in the time domain $s_{u_{(g)}, v_g}(t)$ can be written as [1]:

$$\begin{aligned} s_{u_{(g)}, v_g}(t) &= \\ \beta_g^{(\text{RA})} \sum_{\nu=0}^{\ell-1} X_{u_{(g)}, v_g}[\nu] e^{j2\pi(\nu + Kk_1 + \bar{k})\Delta f^{(\text{RA})}(t - t^{(\text{CP})} - t_{\text{start}})}, \end{aligned} \quad (11)$$

with

$$\begin{aligned} K &= \Delta f^{(\text{PUSCH})} / \Delta f^{(\text{RA})}, \\ t_{\text{start}} &\leq t < t_{\text{start}} + (N_u + N_{\text{CP}})T_c, \end{aligned}$$

where $\Delta f^{(\text{RA})}$ and $\Delta f^{(\text{PUSCH})}$ are the SCS of the PRACH and Physical Uplink Shared Access Channel (PUSCH) respectively; k_1 is the starting subcarrier index, \bar{k} is a default value that depends on the format and controls the repetitions of the sequence, t_{start} adjusts the start of the preamble to its starting symbol, N_u is the useful number of samples, N_{CP} is the CP number of samples, T_c is the time unit for 5G NR (sampling period), $t^{(\text{CP})}$ is the CP duration computed as $N_{\text{CP}}T_c$, and $\beta_g^{(\text{RA})}$ is the amplitude scaling factor in order to conform to the transmit power [16]. We assume perfect open-loop power control and time-alignment.

B. Channel model

Each device transmits the preamble signal over an independent channel to the $n^{(\text{ant})}$ receiving antennas at the gNB. We assume a flat-fading channel, implying that channel gains remain constant across the ℓ allocated subcarriers, that is, the coherence bandwidth encompasses all the subcarriers used to transmit the sequence. For the g -th device, the channel toward the i -th antenna during the m -th repetition is denoted by $h_g^{m,i}$. The vector containing the channel realizations for all active users at the considered PRACH occasion is given by \mathbf{h} . We assume channel realizations to be independent across devices and antennas, that is, $h_g^{m,i} \perp\!\!\!\perp h_g^{m,i'} \perp\!\!\!\perp h_{g'}^{m,i}$. However, we consider two key cases depending on the coherence time across repetitions:

- Independent channel realizations at different repetitions $h_g^{m,i} \perp\!\!\!\perp h_g^{m',i}$.
- Identical channel realizations at different repetitions, that is, the coherence time is longer than the duration of the whole PRACH sequence and repetitions $h_g^{m,i} = h_g^{m',i}$.

Moreover, we model the channel's possible Doppler shift as a CFO between the transmitter and the receiver, which shifts the signal in frequency. Each device suffers a different CFO, $\epsilon_g = \frac{\Delta f_g}{\Delta f^{(\text{RA})}}$, where ϵ_g is the normalized CFO and Δf_g is the absolute frequency offset of device g . We name the set of all CFOs as $\epsilon = \{\epsilon_1, \dots, \epsilon_{n^{(\text{dev})}}\}$.

Under ideal power control assumption, all links can be modeled as complex Gaussian channels with equal power,

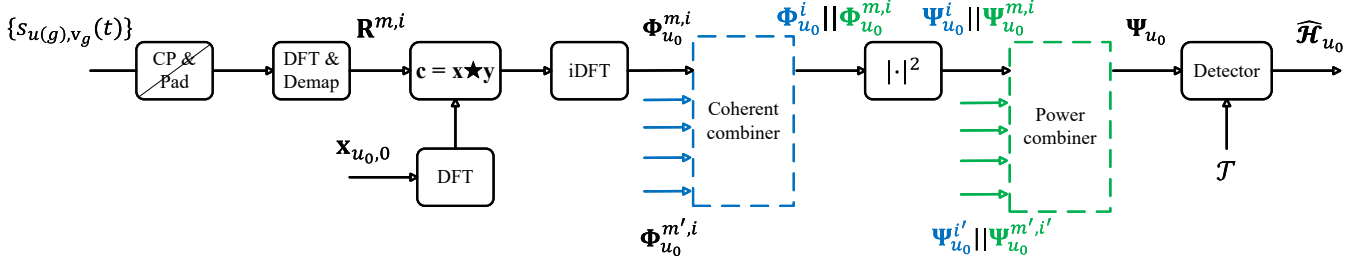


Fig. 2. Full frequency domain representation of the PRACH receiver.

$h_g^{m,i} \sim \mathcal{CN}(0, \sigma_h^2)$. For convenience, we normalize the channel to $\sigma_h^2 = 1$ without loss of generality. The noise at each receiving antenna is modeled as $w^{m,i} \sim \mathcal{CN}(0, \sigma_w^2)$. Accordingly, the per-antenna signal to noise ratio (SNR) is $\frac{1}{2\sigma_w^2}$. We also assume that all devices are sufficiently synchronized to remain within the receiving window, and that any residual delay can be absorbed as a phase shift in the channel response.

C. PRACH receiver

Fig. 2 illustrates the representation of the PRACH processing for i -th antenna, m -th repetition, and root u_0 under test. First, both the CP and padding are removed from the received signal. Then, the subcarriers corresponding to the ZC sequence are demapped via the DFT. Next, cross-correlation is performed between the received sequence and the reference sequence associated with the root configured at the gNB. If there is more than one antenna or sequence repetition, a signal combination is applied that may be coherent or power-based. Finally, a threshold-based detector determines whether a signal has been transmitted.

To facilitate analysis and without loss of generality, we assume $k_1 = 0$ in eq. (11), which implies that the preamble is transmitted in the first set of Physical Resource Blocks (PRBs). Furthermore, since we assume that the channel gains of ℓ subcarriers are equal, as we consider a flat fading channel, the aggregated received signal from all users can be written in the frequency domain as:

$$R^{m,i}[\nu] = \sum_{g=1}^{n^{(\text{dev})}} H_g^{m,i} X_{u(g),v_g}[\nu] + W^{m,i}[\nu]. \quad (12)$$

where $W^{m,i}[\nu]$ is the additive noise term in frequency; $X_{u(g),v_g}[\nu]$ is the ν -th element of the sequence transmitted by the g -th user in the frequency domain; and $H_g^{m,i}$ denotes the channel frequency response from the g -th user to the i -th antenna during repetition m .

The correlation at each antenna i and repetition m between the received signal and the reference sequence for the evaluated root (u_0 without loss of generality) is denoted as $\Phi_{u_0}^{m,i}[k]$. Instead of evaluating different correlations for all CS sequences, it is evaluated in the frequency domain with the reference sequence at zero delay, $X_{u_0,0}$, and the whole vector of correlations is kept after the iDFT.

Then, taking into account the linearity of iDFT as well as the circular correlation, $\Phi_{u_0}^{m,i}[k]$ can be written as [12]:

$$\Phi_{u_0}^{m,i}[k] = \mu_{u_0}^{m,i}[k](\mathbf{h}) + z^{m,i}[k]; k = 0, \dots, \ell - 1 \quad (13)$$

being

$$\mu_{u_0}^{m,i}[k](\mathbf{h}) = \sum_{g \in \mathcal{D}} h_g^{m,i} c_{u(g),v_g,u_0,0}^{\epsilon_g}[k], \quad (14)$$

with $z^{m,i}[k] = \frac{1}{\ell} \sum_{n=0}^{\ell-1} w^{m,i}[n] x_{u_0,0}^*[n-k]$ complex Gaussian noise, $z^{m,i}[k] \sim \mathcal{CN}(0, \sigma_w^2/\ell)$, and $c_{u(g),v_g,u_0,0}^{\epsilon_g}[k]$ the correlation of the reference signal with that transmitted by the g -th device and shifted in frequency ϵ_g as given in eq. (9).

D. Decision statistic

The different behavior in $\Phi_{u_0}^{m,i}[k]$ enables distinguishing whether there exists a user that has been transmitting with the u_0 root and cyclic shift κ_v . As a set of $n^{(\text{rep})}n^{(\text{ant})}$ correlations are available, one per antenna and repetition, the output of the correlators are combined to obtain a single decision statistic. That combination can be done in several forms.

1) *Power combining (PC)*: The power of the correlation or power delay profile (PDP) of the preamble per antenna and repetition is combined to make the decision as (green block in Fig. 2):

$$\Psi_{u_0}^{(p)}[k] = \sum_{i=1}^{n^{(\text{ant})}} \sum_{m=1}^{n^{(\text{rep})}} |\Phi_{u_0}^{m,i}[k]|^2. \quad (15)$$

2) *Coherent combining (CC)*: As PC loses the phase information in $\Phi_{u_0}^{m,i}[k]$, a coherent combining of the repetitions is done before evaluating the absolute value, in a mixed form (blue block in Fig. 2):

$$\Psi_{u_0}^{(c)}[k] = \sum_{i=1}^{n^{(\text{ant})}} \left| \sum_{m=1}^{n^{(\text{rep})}} \Phi_{u_0}^{m,i}[k] \right|^2. \quad (16)$$

This option takes advantage of correlation in the time domain for channel realizations and of independence in the antenna domain.

E. Hypothesis test and design criteria

The selected combined statistic $\Psi_{u_0}[k]$ is employed to distinguish between two actual hypotheses: \mathcal{H}_1 if a user is using root u_0 and cyclic shift κ_v ; and \mathcal{H}_0 in case of no such PRACH transmission. Consequently, we have two possible decisions, named $\hat{\mathcal{H}}_0$ and $\hat{\mathcal{H}}_1$, taken as $\Phi_{u_0} \in Z_0$ or Z_1 , where Z_0, Z_1 are the decision regions to be designed. The performance requirement of PRACH for preamble detection is determined by these two parameters:

- False alarm (fa): is defined as a conditional total probability of erroneous detection of the preamble when the input is only noise, evaluated as:

$$p^{(\text{fa})}(Z_1) = \Pr \left\{ \widehat{\mathcal{H}}_1 | \mathcal{H}_0 \right\}. \quad (17)$$

- True detection (td): is defined as the conditional probability of detection of the preamble when the signal is present:

$$p^{(\text{td})}(Z_1) = \Pr \left\{ \widehat{\mathcal{H}}_1 | \mathcal{H}_1 \right\}. \quad (18)$$

The standard fixes a maximum false alarm probability, $p^{(\text{fa_des})}$, for specific PRACH formats, channel models, and SNR points [19]. Consequently, the design must detect as many device accesses as possible, while keeping the probability of false alarms limited, designing Z_1 such as:

$$\begin{aligned} \max_{Z_1} p^{(\text{td})}(Z_1) \\ \text{s.t. } p^{(\text{fa})}(Z_1) \leq p^{(\text{fa_des})} \end{aligned} \quad (19)$$

Since we have combined the PRACH signal from multiple antennas and sequences to reduce it to a single statistical decision, the decision region Z_1 translates into calculating a threshold \mathcal{T} , as shown in Fig. 2:

$$\Psi_{u_0}[k] \underset{\widehat{\mathcal{H}}_0}{\overset{\widehat{\mathcal{H}}_1}{\gtrless}} \mathcal{T}. \quad (20)$$

Note that there is a trade-off, as attempting to reduce the probability of false alarm will always lead to a deterioration in the probability of detection, and vice versa.

IV. PROBABILISTIC ANALYSIS

In order to design a detector, the transition probabilities, that is, the distributions for the vector Ψ_{u_0} have to be evaluated. It is clear from eq. (13) that $\Phi_{u_0}^{m,i}[k]$ conditioned on \mathbf{h} (explicitly indicated by including \mathbf{h} in the description) are $n^{(\text{ant})}n^{(\text{rep})}$ complex Gaussian random variables, each with its own average and the same variance:

$$\Phi_{u_0}^{m,i}[k](\mathbf{h}) \sim \mathcal{CN}(\mu_{u_0}^{m,i}[k](\mathbf{h}), \sigma_z^2). \quad (21)$$

The output of the combiner for a given channel sample would always results in the sum of Gaussian variables with a mean different from 0, which are subsequently squared. It is well known that this squaring yields a scaled non-central χ^2 distribution, commonly notated as χ'^2 [20]. The non-centrality parameter $\lambda_{u_0}[k](\mathbf{h})$ is distributed as a mix of linear and squared combinations of channel samples.

As $h_g^{m,i}$ are complex Gaussian variables, their weighted combinations in eq. (14) can be also described as Gaussian after deconditioning on \mathbf{h} :

$$\mu_{u_0}^{m,i}[k](\mathbf{h}) \sim \mathcal{CN}(0, \sigma_{u_0}^2[k]), \quad (22)$$

with

$$\sigma_{u_0}^2[k] = \sigma_h^2 \sum_{g \in \mathcal{D}} \left| c_{u(g), v_g, u_0, 0}^{\epsilon_g}[k] \right|^2. \quad (23)$$

The variance $\sigma_{u_0}^2[k]$ depends on the set of transmitting devices for each PRACH occasion, the roots and the CSs they are using, as well as the undergoing CFOs:

- Under \mathcal{H}_0 , the received signal does not include any device transmission for the root u_0 , but it might contain interference from other roots; thus:

$$\hat{\sigma}_{u_0}^2[k] = \sigma_h^2 \sum_{g \in \mathcal{D}_{u_0}} \left| c_{u(g), v_g, u_0, 0}^{\epsilon_g}[k] \right|^2, \quad (24)$$

- Under \mathcal{H}_1 , the received signal also includes the transmitted signal for CS κ_v and root u_0 ; thus, for that specific cyclic shift:

$$\check{\sigma}_{u_0}^2[k] = \sigma_h^2 |c_{u_0, v, u_0, 0}^{\epsilon_0}[k]|^2 + \hat{\sigma}_{u_0}^2[k]. \quad (25)$$

As we obtain the statistics, we will use $\sigma_{u_0}^2$ as any one of them.

A. Power combining (PC)

Conditioned on channel samples, all realizations of $\Phi_{u_0}^{m,i}[k]$ are independent; thus, $\Psi_{u_0}^{(\text{p})}[k]$ in eq. (15) is the addition of the absolute value squared of the $n^{(\text{ant})}n^{(\text{rep})}$ variables following the Gaussian distribution in eq. (21), which is the scaled χ'^2 distribution that can be expressed as:

$$\Psi_{u_0}^{(\text{p})}[k](\mathbf{h}) \sim \sigma_z^2 \chi'_{2n^{(\text{ant})}n^{(\text{rep})}} \left(\frac{\lambda_{u_0}^{(\text{p})}[k](\mathbf{h})}{\sigma_z^2} \right), \quad (26)$$

with the non-centrality parameter given by

$$\lambda_{u_0}^{(\text{p})}[k](\mathbf{h}) = \sum_{i=1}^{n^{(\text{ant})}} \sum_{m=1}^{n^{(\text{rep})}} |\mu_{u_0}^{m,i}[k](\mathbf{h})|^2. \quad (27)$$

As previously described, two key cases for the distribution of the channel samples have been evaluated:

1) *Independent channel realizations per repetition:* We assume each repetition sees an independent channel realization. Thus, $\lambda_{u_0}^{(\text{p})}[k]$ is the addition of the squared absolute value of independent complex Gaussian variables, i.e., a χ^2 distribution: $\lambda_{u_0}^{(\text{p})}[k](\mathbf{h}) \sim \frac{\sigma_{u_0}^2[k]}{2} \chi_{2n^{(\text{ant})}n^{(\text{rep})}}^2$.

As detailed in the Appendix, the marginal distribution of a scaled χ'^2 distribution (eq. 26) with the non-centrality parameter following a scaled χ^2 distribution with the same degrees of freedom (DOF) is also a χ^2 distribution with the same DOF. Thus, the distribution for combination is:

$$\dot{\Psi}_{u_0}^{(\text{p})}[k] \sim \sigma_z^2 \left(1 + \frac{\sigma_{u_0}^2[k]}{2\sigma_z^2} \right) \chi_{2n^{(\text{ant})}n^{(\text{rep})}}^2. \quad (28)$$

with the dot above the variable indicating the distribution under independent channel realizations. Its complementary cumulative distribution function (CCDF) can be expressed following eq. (60) of Appendix as:

$$\bar{F}_{\dot{\Psi}_{u_0}^{(\text{p})}[k]}(\psi) = \frac{\Gamma \left(n^{(\text{ant})}n^{(\text{rep})}, \frac{\psi}{2\sigma_z^2 + \sigma_{u_0}^2[k]} \right)}{\Gamma(n^{(\text{ant})}n^{(\text{rep})})}. \quad (29)$$

It is important to note that $\sigma_{u_0}^2[k]$ can represent $\hat{\sigma}_{u_0}^2[k]$ or $\check{\sigma}_{u_0}^2[k]$ depending on whether the CCDF is conditioned on \mathcal{H}_0 or \mathcal{H}_1 , respectively.

2) *Identical channel realizations per repetition*: In this other key case, the different repetitions are carried out over identical channel realizations, then the non-centrality parameter can be expressed as:

$$\ddot{\lambda}_{u_0}^{(p)}[k](\mathbf{h}) = n^{(\text{rep})} \sum_{i=1}^{n^{(\text{ant})}} |\mu_{u_0}^{1,i}[k](\mathbf{h})|^2. \quad (30)$$

As channel realizations between antennas are independent, $\sum_{i=1}^{n^{(\text{ant})}} |\mu_{u_0}^{1,i}[k](\mathbf{h})|^2 \sim \frac{\sigma_{u_0}^2[k]}{2} \chi_{2n^{(\text{ant})}}^2$, with $\sigma_{u_0}^2[k]$ still given by eq. (23). Therefore, the non-centrality parameter distribution can be described as $\ddot{\lambda}_{u_0}^{(p)}[k](\mathbf{h}) \sim n^{(\text{rep})} \frac{\sigma_{u_0}^2[k]}{2} \chi_{2n^{(\text{ant})}}^2$.

Again, we have the χ'^2 in eq. (26) conditioned on a χ^2 distribution but now the DOF are different for both variables. Thus, as shown in the Appendix, the distribution can be written as the convolution of two χ^2 distributions:

$$\ddot{\Psi}_{u_0}^{(p)}[k] \sim \sigma_z^2 \chi_{2n^{(\text{ant})}(n^{(\text{rep})}-1)}^2 * \sigma_z^2 \left(1 + \frac{n^{(\text{rep})} \sigma_{u_0}^2[k]}{2\sigma_z^2} \right) \chi_{2n^{(\text{ant})}}^2. \quad (31)$$

where $*$ is the convolution operator and the double dot above the variable indicates the distribution under identical channel realizations.

Consequently, its CCDF can be expressed following eq. (59) of Appendix:

$$\begin{aligned} \bar{F}_{\ddot{\Psi}_{u_0}^{(p)}[k]}(\psi) &= 1 - \sum_{j=0}^{\infty} \frac{\Gamma(j+n^{(\text{ant})})}{j! \Gamma(n^{(\text{ant})})} \left(\frac{\sigma_{\theta}^2[k]}{\sigma_{\theta}^2[k]+1} \right)^j \\ &\quad \left(\frac{1}{\sigma_{\theta}^2[k]+1} \right)^{n^{(\text{ant})}} \frac{\gamma(n^{(\text{ant})}n^{(\text{rep})}+j, \frac{\psi}{2\sigma_z^2})}{\Gamma(n^{(\text{ant})}n^{(\text{rep})}+j)}, \end{aligned} \quad (32)$$

where $\sigma_{\theta}^2[k] = n^{(\text{rep})} \sigma_{u_0}^2[k]/2\sigma_z^2$.

B. Coherent combining (CC)

This scheme performs a coherent combining of the repetitions before evaluating the absolute value, to subsequently combine by antenna. In this case, the inner sum of the absolute value of eq. (16) for each antenna follows the next distribution:

$$\sum_{m=1}^{n^{(\text{rep})}} \Phi_{u_0}^{m,i}[k](\mathbf{h}) \sim \mathcal{CN} \left(\sum_{m=1}^{n^{(\text{rep})}} \mu_{u_0}^{m,i}[k](\mathbf{h}), n^{(\text{rep})} \sigma_z^2 \right). \quad (33)$$

As before, conditioned on channel samples, all the antenna channel realizations are independent; then, $\Psi_{u_0}^{(c)}[k]$ in eq. (16) is the addition of the square of the absolute value of $n^{(\text{ant})}$ variables following the Gaussian distribution in eq. (33), which is the following scaled χ'^2 distribution:

$$\Psi_{u_0}^{(c)}[k] \sim n^{(\text{rep})} \sigma_z^2 \chi_{2n^{(\text{ant})}}'^2 \left(\frac{\lambda_{u_0}^{(c)}[k](\mathbf{h})}{n^{(\text{rep})} \sigma_z^2} \right), \quad (34)$$

with non-centrality parameter:

$$\lambda_{u_0}^{(c)}[k](\mathbf{h}) = \sum_{i=1}^{n^{(\text{ant})}} \left| \sum_{m=1}^{n^{(\text{rep})}} \mu_{u_0}^{m,i}[k](\mathbf{h}) \right|^2. \quad (35)$$

Next, the same two key cases have been evaluated.

1) *Independent channel realizations per repetition*: Now, the additions within $\lambda_{u_0}^{(c)}[k]$ in eq. (35) are all independent; thus, the marginal distribution of the inner sum for each antenna is given by: $\sum_{m=1}^{n^{(\text{rep})}} \mu_{u_0}^{m,i}[k](\mathbf{h}) \sim \mathcal{CN}(0, n^{(\text{rep})} \sigma_{u_0}^2[k])$. Therefore, $\lambda_{u_0}^{(c)}[k]$ is distributed as the addition of $2n^{(\text{ant})}$ Gaussian variables with 0 mean and $n^{(\text{rep})} \sigma_{u_0}^2[k]$ variance; thus, $\lambda_{u_0}^{(c)}[k] \sim n^{(\text{rep})} \frac{\sigma_{u_0}^2[k]}{2} \chi_{2n^{(\text{ant})}}^2$.

Consequently, we have again a scaled χ'^2 distribution with a scaled χ^2 as a non-centrality parameter, both with two DOF. Therefore, the marginal distribution can be expressed as:

$$\ddot{\Psi}_{u_0}^{(c)}[k] \sim n^{(\text{rep})} \sigma_z^2 \left(1 + \frac{\sigma_{u_0}^2[k]}{2\sigma_z^2} \right) \chi_{2n^{(\text{ant})}}^2, \quad (36)$$

with its corresponding CCDF as eq. (60) of Appendix:

$$\bar{F}_{\ddot{\Psi}_{u_0}^{(c)}[k]}(\psi) = \frac{\Gamma(n^{(\text{ant})}, \frac{\psi}{2n^{(\text{rep})} \sigma_z^2 + n^{(\text{rep})} \sigma_{u_0}^2[k]})}{\Gamma(n^{(\text{ant})})}. \quad (37)$$

2) *Identical channel realizations per repetition*: Now, as the different repetitions has the same channel realization, the non-centrality parameter in eq. (35) can be expressed as $\ddot{\lambda}_{u_0}^{(c)}[k](\mathbf{h}) = \sum_{i=1}^{n^{(\text{ant})}} |n^{(\text{rep})} \mu_{u_0}^i[k](\mathbf{h})|^2$, which, since channel realizations between antennas are independent, follows the distribution $\ddot{\lambda}_{u_0}^{(c)}[k](\mathbf{h}) \sim (n^{(\text{rep})})^2 \frac{\sigma_{u_0}^2[k]}{2} \chi_{2n^{(\text{ant})}}^2$.

Then, $\ddot{\Psi}_{u_0}^{(c)}[k]$ is a scaled χ'^2 with a scaled χ^2 both with two DOF, that as we have seen before, can be expressed as:

$$\ddot{\Psi}_{u_0}^{(c)}[k] \sim n^{(\text{rep})} \sigma_z^2 \left(1 + \frac{n^{(\text{rep})} \sigma_{u_0}^2[k]}{2\sigma_z^2} \right) \chi_{2n^{(\text{ant})}}^2, \quad (38)$$

with CCDF:

$$\bar{F}_{\ddot{\Psi}_{u_0}^{(c)}[k]}(\psi) = \frac{\Gamma(n^{(\text{ant})}, \frac{\psi}{2n^{(\text{rep})} \sigma_z^2 + (n^{(\text{rep})})^2 \sigma_{u_0}^2[k]})}{\Gamma(n^{(\text{ant})})}. \quad (39)$$

V. OPTIMAL DETECTOR WITHOUT CFO

In this section, we define the optimal detector for the absence of CFO. This is based on the premise that the correlation of a sequence with the same root as the reference is zero, except at the CS of the transmitted device κ_{v_g} , since there is no power transfer between correlation lags k , while the effects of other roots can be considered as an increase in the noise level.

Considering this case, the correlation values simplify to those of eq. (5) and (6), while $\sigma_{u_0}^2$ can be expressed as:

- Under \mathcal{H}_0 :

$$\hat{\sigma}_{u_0}^2 = \sigma_h^2 \sum_{g \in \mathcal{D}_{u_0}} \frac{1}{\ell} = \sigma_h^2 \frac{n_{u_0}^{(\text{inter})}}{\ell}, \quad (40)$$

- Under \mathcal{H}_1 :

$$\hat{\sigma}_{u_0}^2 = \sigma_h^2 \left(1 + \frac{n_{u_0}^{(\text{inter})}}{\ell} \right). \quad (41)$$

where $n_{u_0}^{(\text{inter})} = n^{(\text{dev})} - n_{u_0}^{(\text{dev})}$ is the number of devices transmitting using a different root than the reference. Note that $\hat{\sigma}_{u_0}^2$ and $\check{\sigma}_{u_0}^2$ do not depend on the lag k , simplifying the analysis as all lags exhibit the same variance.

A false alarm might occur with probability $p_{u_0}^{(\text{fa})}[k](\mathcal{T}) = \Pr\{\Psi_{u_0}[k] > \mathcal{T}|\mathcal{H}_0\} = \bar{F}_{\Psi_{u_0}[k]|\mathcal{H}_0}(\mathcal{T})$, that is, the false alarm is given by the CCDF for $\Psi_{u_0}[k]$ conditioned on no PRACH transmission for the root and CS under test. On the other hand, a true detection would happen with probability $p_{u_0}^{(\text{td})}[k](\mathcal{T}) = \Pr\{\Psi_{u_0}[k] > \mathcal{T}|\mathcal{H}_1\} = \bar{F}_{\Psi_{u_0}[k]|\mathcal{H}_1}(\mathcal{T})$.

As a design criterion, assuming that the devices on each PRACH occasion randomly select CSs among all configured roots, we can assume that the mean of $n_{u_0}^{(\text{inter})}$ is the same for all roots. Furthermore, since the channel is flat and the circular correlation between sequences with the same root is a Kronecker delta, while that between different roots is a constant, we can consider all roots and cyclic shift as equivalent. In this way, the same threshold can be used for all roots configured in the gNB. A false alarm might occur in any root, thus, in order to keep the false alarm rate below the maximum, $p^{(\text{fa})}(\mathcal{T}) \leq p^{(\text{fa_des})}$, the test for each root and correlation lag k should be kept below a value $p^{(\text{fa_sample_des})}$, which is the desired probability of false alarm per lag and per root, easily obtained assuming independence among samples. Consequently, we can obtain the optimal threshold for both signal combiners solving the following equation:

$$p^{(\text{fa_sample_des})} = 1 - \left(1 - p^{(\text{fa_des})}\right)^{\frac{1}{n^{(\text{root})}_\ell}} = \bar{F}_{\Psi_{u_0}[k]|\mathcal{H}_0}(\mathcal{T}). \quad (42)$$

A. Optimal threshold for PC

1) *Independent channel realizations per repetition*: As described above, the optimal threshold is obtained by solving eq. (42), using the CCDF described in eq. (29) conditioned on the \mathcal{H}_0 hypothesis, that is, with $\hat{\sigma}_{u_0}^2$ defined in eq. (40):

$$\dot{\mathcal{T}}_{u_0}^{(\text{p})} = (2\sigma_z^2 + \hat{\sigma}_{u_0}^2) \Gamma^{(\text{inv})} \left(n^{(\text{ant})} n^{(\text{rep})}, p^{(\text{fa_sample_des})} \right), \quad (43)$$

where $\Gamma^{(\text{inv})}$ is the inverse of the upper incomplete Gamma function.

Given that $\hat{\sigma}_{u_0}^2$ depends on $n_{u_0}^{(\text{inter})}$, $\dot{\mathcal{T}}_{u_0}^{(\text{p})}$ is an instantaneous threshold whose value would have to be updated in each PRACH occasion. Since $n_{u_0}^{(\text{inter})}$ is unknown a priori, the mean of its distribution based on cell traffic could be used instead, in which case we would have an average threshold to achieve the target false alarm over a period of time. This approach is also valid, as the standard dictates that it must be statistically fulfilled.

Following, the true detection probability can also be obtained under \mathcal{H}_1 hypothesis plugging the calculated threshold in eq. (29) while the variance is $\check{\sigma}_{u_0}^2$ defined in eq. (41):

$$\dot{p}^{(\text{td})}(\text{p})[\dot{\mathcal{T}}_{u_0}^{(\text{p})}] = \frac{\Gamma \left(n^{(\text{ant})} n^{(\text{rep})}, \frac{\dot{\mathcal{T}}_{u_0}^{(\text{p})}}{2\sigma_z^2 + \check{\sigma}_{u_0}^2} \right)}{\Gamma \left(n^{(\text{ant})} n^{(\text{rep})} \right)}. \quad (44)$$

2) *Identical channel realizations per repetition*: The threshold, $\check{\mathcal{T}}_{u_0}^{(\text{p})}$, can be obtained from the CCDF in eq. (32) under the \mathcal{H}_0 hypothesis. In this case, there is no closed-form for the optimal threshold, since the function has no inverse, but the value is easily obtained with numerical methods as the CCDF is monotonically growing. Finally, the detection probability can be expressed as: $\dot{p}^{(\text{td})}(\text{p})[\check{\mathcal{T}}_{u_0}^{(\text{p})}] = \bar{F}_{\check{\Psi}_{u_0}^{(\text{p})}[k]|\mathcal{H}_1}(\check{\mathcal{T}}_{u_0}^{(\text{p})})$.

B. Optimal threshold for CC

1) *Independent channel realizations per repetition*: Following the same steps as before, the optimal threshold is determined solving eq. (42), using the CCDF in eq. (39) conditioned on \mathcal{H}_0 hypothesis:

$$\dot{\mathcal{T}}_{u_0}^{(\text{c})} = n^{(\text{rep})} (2\sigma_z^2 + \hat{\sigma}_{u_0}^2) \Gamma^{(\text{inv})} \left(n^{(\text{ant})}, p^{(\text{fa_sample_des})} \right).$$

On the other hand, the detection probability can be obtained as $\dot{p}^{(\text{td})}(\text{c})[\dot{\mathcal{T}}_{u_0}^{(\text{c})}] = \bar{F}_{\dot{\Psi}_{u_0}^{(\text{c})}[k]|\mathcal{H}_1}(\dot{\mathcal{T}}_{u_0}^{(\text{c})})$ under \mathcal{H}_1 hypothesis.

2) *Identical channel realizations per repetition*: In a similar way to the previous case, the optimal threshold would be:

$$\dot{\mathcal{T}}_{u_0}^{(\text{c})} = n^{(\text{rep})} \left(2\sigma_z^2 + n^{(\text{rep})} \hat{\sigma}_{u_0}^2 \right) \Gamma^{(\text{inv})} \left(n^{(\text{ant})}, p^{(\text{fa_sample_des})} \right),$$

and the corresponding detection probability computed as $\dot{p}^{(\text{td})}(\text{c})[\dot{\mathcal{T}}_{u_0}^{(\text{c})}] = \bar{F}_{\dot{\Psi}_{u_0}^{(\text{c})}[k]|\mathcal{H}_1}(\dot{\mathcal{T}}_{u_0}^{(\text{c})})$.

VI. DETECTOR DESIGN WITH CFO

We modify the detection algorithm to include the possibility of CFO. We assume PC and independent channel realizations per repetition for simplicity, as CC and equal channel realizations can be added as in the previous analysis.

When the signal is affected by CFO, part of the signal power is spread over all correlation lags, creating non-uniform intra-root interference. In the case of $\epsilon < 0.5$, this interference is distributed in descending order across the lags, maintaining a constant distance between them with respect to the transmitted preamble. Fig. 3 shows an example without noise or channel effects of format C0 with $\epsilon = 0.3$ and reference root $u_0 = 51$. This inter-sample distance can be calculated as [8]:

$$d = \begin{cases} d_u & \text{if } 0 \leq d_u < \ell/2 \\ \ell - d_u & \text{if } d_u \geq \ell/2 \end{cases} \quad (45)$$

where d_u is the smallest non-negative integer satisfying $(u \cdot d_u)_\ell = 1$. It can be seen that the true peak produces false peaks with a smaller amplitude as the distance increases. Consequently, the lag order from largest to smallest PDP amplitude is $(\kappa_v + b \cdot d)_\ell$, where $b \in \mathbb{Z}$.

In the presence of channel and noise, it may happen that one of these false peaks has a higher amplitude than the true peak. Therefore, the possible events that can trigger a false alarm if the above detector is used are:

- Noise plus interference from other roots causes a sample exceed the threshold \mathcal{T} .
- If there is a true peak at $k^{(\text{t})}$ which gives rise to a false peak at $k^{(\text{f})} = (k^{(\text{t})} + b \cdot d)_\ell$, which is greater than \mathcal{T} .

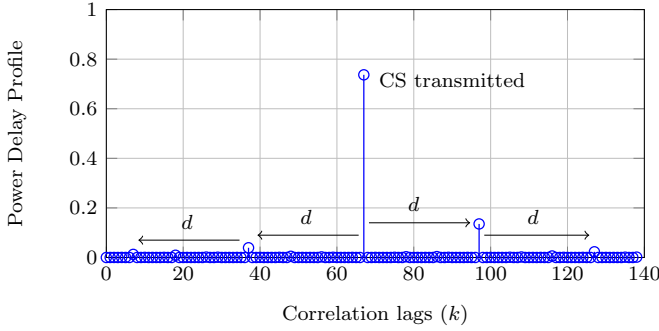


Fig. 3. Format C0 PDP with $\epsilon = 0.3$ and $u_0 = 51$ without noise and channel.

This produces a false alarm in $k^{(f)}$ whether or not $k^{(t)}$ is detected.

This behavior makes the distribution of Ψ dependent on the lag k , and hence on the threshold. As a consequence, the CCDF of $\Psi_{u_0}[k]$ for PC follows eq. (29) and its threshold can be expressed for the reference root u_0 as:

$$\dot{\mathcal{T}}_{u_0}^{(\text{CFO})}[k] = \frac{\Gamma^{(\text{inv})}(n^{(\text{ant})}n^{(\text{rep})}, p^{(\text{fa_sample_des})})}{(2\sigma_z^2 + \sigma_{u_0}^2[k])^{-1}}, \quad (46)$$

where $\sigma_{u_0}^2[k]$ follows eq. (23).

As above, the total probability of false alarm will be:

$$\dot{p}^{(\text{fa})} = 1 - \prod_{u \in \mathcal{R}} \prod_{k=0}^{\ell-1} \left(1 - \bar{F}_{\dot{\Psi}_u[k]}(\dot{\mathcal{T}}_u^{(\text{CFO})}[k])\right), \quad (47)$$

and the true detection probability of the device transmitting at lag $k^{(t)}$:

$$\dot{p}^{(\text{td})(\text{p})}[k^{(t)}] = \bar{F}_{\dot{\Psi}_{u_0}[k^{(t)}]}(\dot{\mathcal{T}}_{u_0}^{(\text{CFO})}[k^{(t)}]). \quad (48)$$

A. Detection algorithm with CFO

Since it is not possible to know in advance which devices will transmit on which CS, the algorithm must be able to locate them and try to avoid selecting false alarms as true peaks. For this purpose, the following algorithm is proposed: If a set of CSs, \mathbf{k}_s , are cyclically separated from each other by $b \cdot d$ samples and exceed the base threshold, $\dot{\mathcal{T}}_{u_0}^{(\text{p})}$, only the highest of them is selected as a true peak and the rest are discarded as false ones. The underlying reasoning takes into account that the highest peak is more likely to be the true one. This process is performed for all the configured roots. In addition, the selected peaks also have to exceed the threshold due to CFO, $\dot{\mathcal{T}}_{u_0}^{(\text{CFO})}[k]$, to ensure that they are not originated due to interference from other roots. The complete algorithm is explained in Algorithm 1.

Using this algorithm, the probability of false alarm will come from the probability of the noise exceeding the threshold and selecting as true detection a false peak originated from the CFO. The probability of selecting a false peak instead of a true one is basically affected by the first false peak, i.e.,

Algorithm 1 Peak Detection and Classification

Ensure: Classified true peaks for all roots.

- 1: **for** each root $u_0 \in \mathcal{R}$ **do**
- 2: Compute the base threshold assuming no CFO as eq. (43)
 $\dot{\mathcal{T}}_{u_0}^{(\text{p})} \leftarrow (2\sigma_z^2 + \hat{\sigma}_{u_0}^2) \Gamma^{(\text{inv})} \left(n^{(\text{ant})}n^{(\text{rep})}, p^{(\text{fa_sample_des})} \right)$
- 3: Find all candidate peak indices
 $\mathbf{k}_{u_0} \leftarrow \{ k \mid \Psi_{u_0}[k] > \dot{\mathcal{T}}_{u_0}^{(\text{p})} \}$
- 4: Initialize classified set $\mathcal{C} \leftarrow \emptyset$
- 5: **while** $\mathbf{k}_{u_0} \setminus \mathcal{C} \neq \emptyset$ **do**
- 6: Select largest remaining peak
 $k_s^{(t)} \leftarrow \arg \max_{k \in \mathbf{k}_{u_0} \setminus \mathcal{C}} \{ \Psi_{u_0}[k] \}$
- 7: Group neighboring peaks at distance $b \cdot d$
 $\mathbf{k}_s \leftarrow \{ (k_s^{(t)} + b \cdot d)_\ell \mid \Psi_{u_0}[(k_s^{(t)} + b \cdot d)_\ell] > \dot{\mathcal{T}}_{u_0}^{(\text{p})} \}$
- 8: Add grouped peaks to classified set: $\mathcal{C} \leftarrow \mathcal{C} \cup \mathbf{k}_s$
- 9: **end while**
- 10: **end for**
- 11: {Interference check}
- 12: **for** each $k_s^{(t)}$ **do**
- 13: Compute interference-aware threshold with CFO,
 $\dot{\mathcal{T}}_{u(s)}^{(\text{CFO})}[k_s^{(t)}]$, based on other true detections
- 14: **if** $\Psi_{u(s)}[k_s^{(t)}] < \dot{\mathcal{T}}_{u(s)}^{(\text{CFO})}[k_s^{(t)}]$ **then**
- 15: Discard $k_s^{(t)}$
- 16: **end if**
- 17: **end for**

$k^{(f)} = (k^{(t)} + d)_\ell$, as it is the highest, and can be expressed for a device g transmitting at the reference root u_0 as:

$$p_g^{(\text{fa_CFO})} = \Pr \left\{ \Psi_{u_0}[k^{(f)}](\mathbf{h}) > \Psi_{u_0}[k^{(t)}](\mathbf{h}) \mid \Psi_{u_0}[k^{(f)}](\mathbf{h}) \geq \tilde{\mathcal{T}}_{u_0}[k^{(f)}] \right\}$$

where $\tilde{\mathcal{T}}_{u_0}[k] = \max(\dot{\mathcal{T}}_{u_0}^{(\text{p})}, \dot{\mathcal{T}}_{u_0}^{(\text{CFO})}[k])$ since if the false peak is selected, then it also has to exceed the threshold due to CFO; and $\Psi_{u_0}[k^{(f)}](\mathbf{h})$ along with $\Psi_{u_0}[k^{(t)}](\mathbf{h})$ follows the distribution of eq. (26).

This probability can be evaluated as the sum of two event probabilities. The first, $p_g^{(1)}$, is the probability that the false peak is higher than the true peak when both peaks exceed the base threshold, so both are detected and the higher one is selected. The second one, $p_g^{(2)}$, is the probability that the false peak exceeds the threshold while the true peak does not (only the false one is selected):

$$p_g^{(\text{fa_CFO})} = p_g^{(1)} + p_g^{(2)}, \quad (49)$$

where $p_g^{(1)}$ can be computed as:

$$\int_{\dot{\mathcal{T}}_{u_0}^{(\text{p})}}^{\infty} \underbrace{\int_{-\infty}^{\infty} \int_{-\infty}^{\infty} \bar{F}_{\Psi_{u_0}[k^{(f)}](\mathbf{h})}(\psi) f_{\Psi_{u_0}[k^{(t)}](\mathbf{h})}(\psi) f_{\mathbf{H}}(\mathbf{h}) d\mathbf{h} d\psi}_{\# \mathbf{h}}$$

and $p_g^{(2)}$ as

$$\int_{-\infty}^{\infty} \int_{-\infty}^{\infty} \bar{F}_{\Psi_{u_0}[k^{(f)}](\mathbf{h})}(\tilde{\mathcal{T}}_{u_0}[k^{(f)}]) F_{\Psi_{u_0}[k^{(t)}](\mathbf{h})}(\dot{\mathcal{T}}_{u_0}^{(\text{p})}) f_{\mathbf{H}}(\mathbf{h}) d\mathbf{h},$$

TABLE II
PRACH FORMAT PARAMETERS [1]

Format	ℓ	PRACH SCS	$n^{(\text{rep})}$	Bandwidth	Duration
0	839	1.25 kHz	1	1.08 MHz	1 ms
C0	139	$15 \cdot 2^\mu$ kHz	1	$2.16 \cdot 2^\mu$ MHz	0.144 ms
B1	139	$15 \cdot 2^\mu$ kHz	2	$2.16 \cdot 2^\mu$ MHz	0.142 ms
B2	139	$15 \cdot 2^\mu$ kHz	4	$2.16 \cdot 2^\mu$ MHz	0.285 ms
B4	139	$15 \cdot 2^\mu$ kHz	12	$2.16 \cdot 2^\mu$ MHz	0.856 ms

Note: $\mu \in \{0, 1, 2, 3\}$ is the numerology parameter.

being $\#\mathbf{h} = n^{(\text{rep})}n^{(\text{ant})}$ the number of elements of \mathbf{h} .

Consequently, the total false alarm probability can be expressed as:

$$p^{(\text{fa})} = p^{(\text{noise_plus_inter})} + \sum_{g \in \mathcal{D}} p_g^{(\text{fa_CFO})}, \quad (50)$$

where $p^{(\text{noise_plus_inter})}$ takes into account that the selected peaks have to exceed both the base threshold and the CFO threshold. It can be expressed following eq. (47) as:

$$p^{(\text{noise_plus_inter})} = 1 - \prod_{u \in \mathcal{R}} \prod_{k=0}^{\ell-1} \left(1 - \bar{F}_{\tilde{\Psi}_u[k]}(\tilde{\mathcal{T}}_u[k]) \right). \quad (51)$$

Moreover, the true detection probability for the device g can be computed as:

$$p_g^{(\text{td})(\text{p})}[k_g^{(t)}] = \bar{F}_{\tilde{\Psi}_{u_0}[k_g^{(t)}]}(\tilde{\mathcal{T}}_{u_0}[k_g^{(t)}]). \quad (52)$$

Knowing the theoretical behavior of the detector allows us to adapt the base threshold, compensating for the CFO effect, and achieve the desired false alarm probability without having a large impact on the detection probability.

VII. NUMERICAL RESULTS

In this section, we evaluate the theoretical expressions derived above for different formats supported in 5G NR as summarized in Table II. All are configured with a 15 kHz SCS, except format 0, which only supports 1.25 kHz, and spread over ℓ subcarriers; thus, all PRACH formats can be assumed to be located within their coherence bandwidth for delay spreads less than or equal to 100 ns. Furthermore, the coherence time for all formats can be guaranteed for frequency Doppler of up to 500 Hz, since their durations are less than 1 ms. In these scenarios, we can assume that the channel realizations per repetition are approximately equal. Additionally, the number of roots configured in gNB are $n^{(\text{root})} = 2$ and the desired maximum $p^{(\text{fa_des})}$ is set to 10^{-3} to determine the optimal threshold for each combination technique.

The closed-form expressions obtained in the previous section have been validated and verified with Monte Carlo simulations. Empirical results were obtained using $6 \cdot 10^5$ PRACH occasions.

A. Signal combiners comparison without CFO

We first consider the no CFO case to compare the performance of different signal combiners. A comparison of the different combination techniques can be seen in Fig. 4

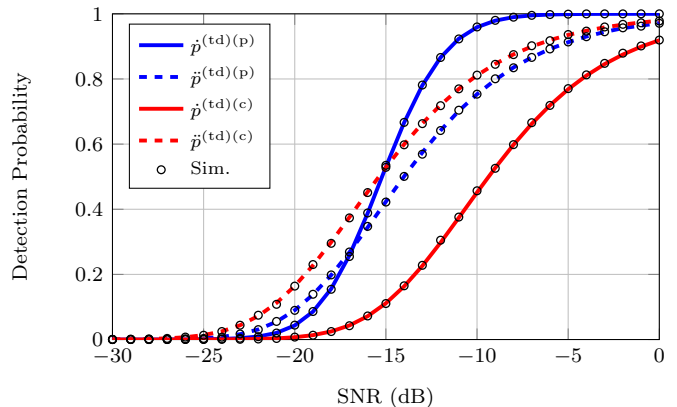


Fig. 4. Detection probability comparison of combining techniques for format B1 with $n^{(\text{ant})} = 1$ and $n^{(\text{inter})} = 0$.

as a function of the SNR per antenna, for B1 format with $n^{(\text{ant})} = 1$ and $n^{(\text{inter})} = 0$. Each combiner computes its optimal threshold based on previous development and measures the detection probability. We observe that CC is the best strategy in the case of identical channel realizations, while PC outperforms CC in the case of independent channel realizations. It is worth noting that, in the low-SNR regime, combiners assuming identical channel realizations perform better than independent ones. This aspect should be considered when designing a low-SNR detector, which will interfere less with other base stations or other configured roots.

Performance also depends on the number of receiving antennas and repetitions. In Fig. 5 we evaluate and compare the performance of the combiners using formats B1 and B2 for a SNR of -20 dB and $n^{(\text{inter})} = 0$. We observe that format B2, which has twice as many repetitions, outperforms format B1 for all combiners, except in the case of CC with independent channel realizations, since in this case the array gain obtained by increasing the number of repetitions is zero. Furthermore, as mentioned above, when dealing with a low-SNR, CC with identical channel realizations outperforms PC until reaching the maximum detection probability. Then, the superiority of CC is also affected by the number of receiving antennas and repetitions. In this case, the largest difference in detection probability for format B1 is found with $n^{(\text{ant})} = 8$, while for format B2 it is with $n^{(\text{ant})} = 4$.

As noted above, combiners are affected by interference from other roots configured in the same gNB. Since $n^{(\text{inter})}$ cannot be known, its average value must be selected based on expected traffic, in order to design the optimal threshold that statistically meets the target $p^{(\text{fa_des})}$. Fig. 6 represents the case of $n^{(\text{inter})} = 1$ for format B1 with $n^{(\text{ant})} = 1$. In PC, interference simply adds extra power (and a small cross-term), raising the noise floor and reducing $p^{(\text{td})}$. Meanwhile, in CC, the interference signal is added to the transmitted signal before squaring. Depending on its phase relative to the transmitted one, it can be combined constructively or destructively. We observe that CC in high-SNR scenarios has a $p^{(\text{td})}$ that is 0.1 lower than that of the case without interference, while PC is only affected in the case of identical channel realizations.

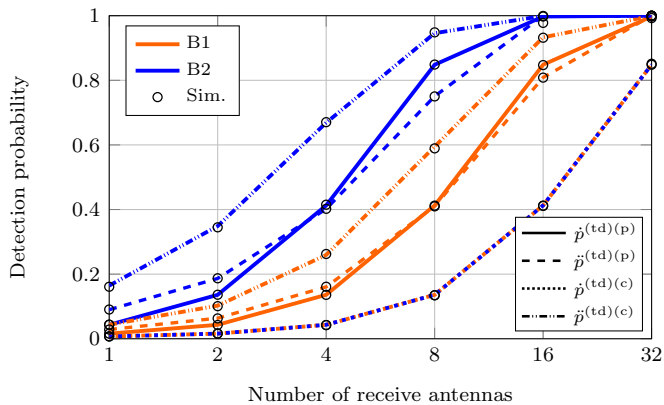


Fig. 5. Detection probability comparison between formats B1 and B2 for different number of receive antennas, SNR of -20 dB, and $n^{(\text{inter})} = 0$.

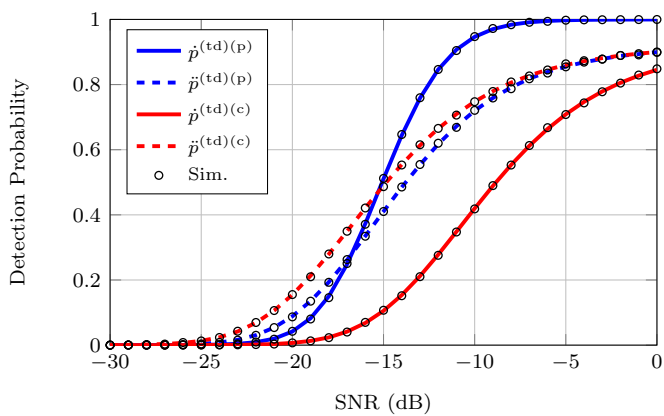


Fig. 6. Detection probability comparison of combining techniques for format B1 with $n^{(\text{ant})} = 1$ and $n^{(\text{inter})} = 1$.

B. Designed algorithm performance with CFO

This subsection validates the algorithm designed in the presence of CFO with PC for formats C0 and 0 with $\epsilon = 0.3$. It is also compared to a *conventional PRACH detector*, whose threshold is computed based on the estimation of the PDP noise floor [21, Ch. 19].

A $p^{(\text{td})}$ comparison between the two formats can be seen in Fig. 7 for different scenarios. We observe that format 0 achieves a better $p^{(\text{td})}$ than format C0 since it has a higher ℓ , collecting more signal power when computing the PDP. On the other hand, we can observe how when introducing CFO, the performance worsens as the threshold has to be increased to maintain the target $p^{(\text{fa})}$, also in the case of interfering devices. Our detector algorithm and the conventional one (conv. det.) obtain similar performance in terms of $p^{(\text{td})}$, since the latter is capable of detecting any peak crossing a threshold. However, it cannot distinguish between true and false peaks originated from CFO, as we will see below.

Figs. 8 and 9 represent the $p^{(\text{fa})}$ of formats C0 and 0, respectively, for different scenarios. In both, the probability remains as desired in the case of no CFO, while with CFO it increases with the SNR up to a certain point and then decreases, making a maximum of $p^{(\text{fa})}$. For the no-interfering case, this effect is

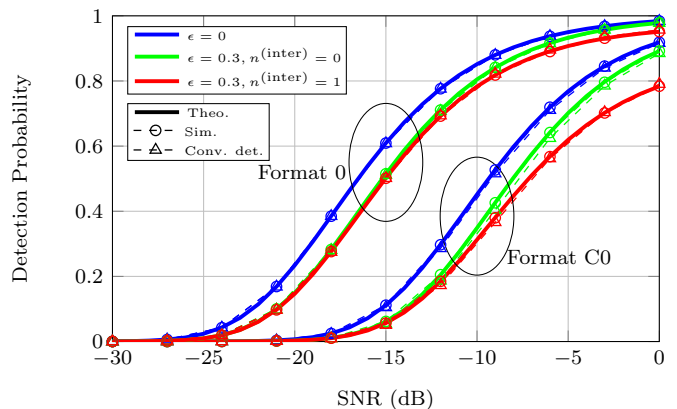


Fig. 7. Detection probability of formats 0 and C0 for the cases of $\epsilon = 0$, $\epsilon = 0.3$, and $\epsilon = 0.3$ with $n^{(\text{inter})} = 1$. Results are compare to a conv. det. [21, Ch. 19].

due to the fact that as SNR increases, the probability of a false peak exceeding the true peak also increases. This effect goes up to a certain SNR beyond which the signal is large enough that the effect of noise can be neglected, and thus the probability returns to the desired level. In the case of interfering devices, it is similar, except that it does not return to the desired level but continues to decrease. As we increase the SNR the base threshold, $\hat{\mathcal{T}}_{u_0}^{(\text{p})}$, starts to become more restrictive than the CFO threshold, $\hat{\mathcal{T}}_{u_0}^{(\text{CFO})}$, removing more noise-detected peaks than necessary to maintain the desired probability. This effect can be mitigated, as observed in the subsequent results.

Note that the nominal frequency offset that each format can tolerate differs greatly. Format 0 with $\epsilon = 0.3$ corresponds to a nominal offset of 375 Hz, which corresponds to a user speed of 120 km/h with a carrier frequency of 3.5 GHz. Whereas, for the format C0 it is 4.5 kHz or the same user speed with a carrier frequency of 40.5 GHz. It is important to note that in both cases the conventional detector cannot maintain the $p^{(\text{fa})}$, since it is not able to distinguish between false and true peaks. The conventional detector increases its $p^{(\text{fa})}$ with SNR until all PRACH occasions result in false alarms.

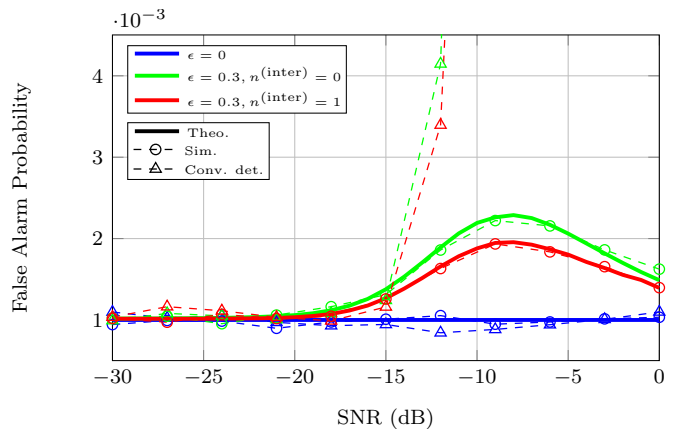


Fig. 8. False alarm probability of format C0 for the cases of $\epsilon = 0$, $\epsilon = 0.3$, and $\epsilon = 0.3$ with $n^{(\text{inter})} = 1$. Results are compare to a conv. det. [21, Ch. 19].

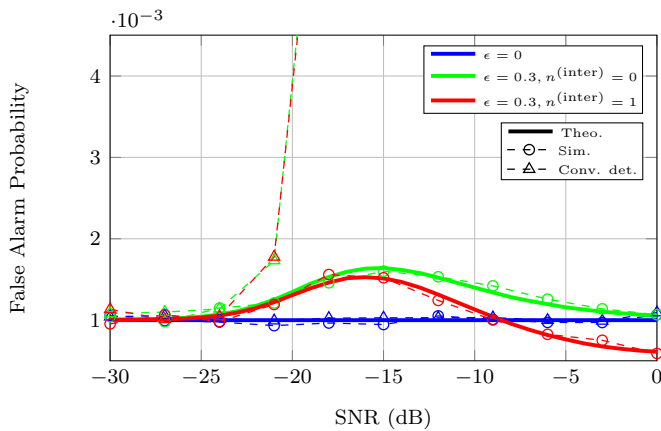


Fig. 9. False alarm probability of format 0 for the cases of $\epsilon = 0$, $\epsilon = 0.3$, and $\epsilon = 0.3$ with $n^{(\text{inter})} = 1$. Results are compare to a conv. det. [21, Ch. 19].

Fig. 10 and 11 show the $p^{(\text{td})}$ and $p^{(\text{fa})}$ of format C0 as the number of antennas increases, with $n^{(\text{inter})} = 1$, respectively. Every time we double the number of antennas, the same $p^{(\text{td})}$ is achieved with a 3 dB lower SNR, exactly matching the expected noise reduction from averaging i.i.d. noise. We also see that the $p^{(\text{fa})}$ due to CFO and its maximum are also reduced. On the other hand, the results of using an adapted base threshold computed by compensating for all the effects introduced by the CFO and the interference are also plotted for the case of $n^{(\text{ant})} = 2$. With this threshold, we can hold $p^{(\text{fa})}$ at its target level without significantly degrading $p^{(\text{td})}$, improving spectral efficiency by reducing the number of attempts required or the reserve of wasted resources.

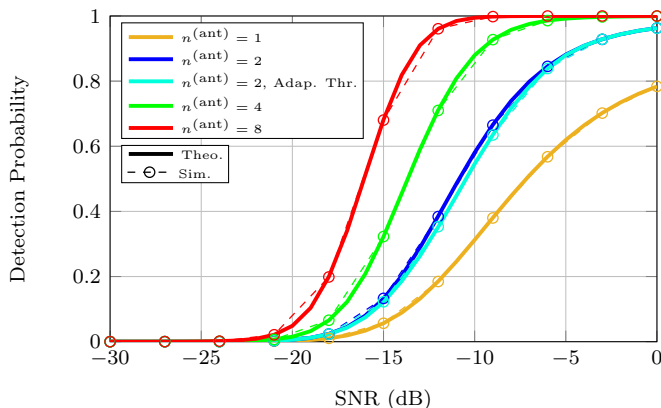


Fig. 10. Detection probability of format C0 for different numbers of received antennas with $n^{(\text{inter})} = 1$. The case of threshold adaptation for 2 antennas is also represented.

VIII. CONCLUSIONS

We have developed and validated a comprehensive statistical framework for 5G-NR PRACH preamble detection and derived closed-form PDP distributions under both hypotheses that account for multiple receive antennas, multiple simultaneous devices, multiple roots, CFO, and two combining methods. We identify two key cases: identical and independent channel

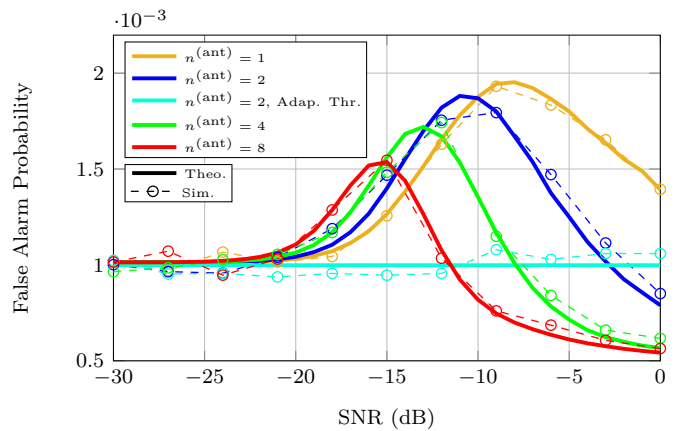


Fig. 11. False alarm probability of format C0 for different numbers of received antennas with $n^{(\text{inter})} = 1$. The case of threshold adaptation for 2 antennas is also represented.

realizations per repetition, that markedly change PRACH performance, and providing threshold expressions dependent on cell traffic to simplify design and analysis. We show that PC is more robust under independent repetition channels and interference, while CC performs best in low-SNR scenarios when repetitions experience identical channels. Finally, we proposed a novel detector with an adaptive threshold that has the same detection capabilities as a conventional detector, while tightly controlling the false alarm probability as desired, and thus its spectral efficiency. The extension of the proposed framework to multipath channels is left for future work, as its exhaustive and comprehensive explanation requires a dedicated study. These results provide both theoretical insight and practical tools for efficient PRACH configuration in dense and heterogeneous 5G deployments.

IX. APPENDIX. USEFUL DISTRIBUTIONS

Random variable (RV) X is distributed following the known distribution D , $X \sim D$, e.g. $X \sim \mathcal{N}(\mu, \sigma^2)$. The probability density function (PDF) is denoted as $f_X(x) = f_D(x)$, the cumulative distribution function (CDF) as $F_X(x) = F_D(x)$, the CCDF as $\bar{F}_X(x) = 1 - F_X(x) = \bar{F}_D(x)$ and the moment generating function (MGF) is $M_X(t) = M_D(t) = \mathbb{E}[\exp(tX)]$. For vectors, each element is distributed according to the distribution, and we assume independence between elements unless otherwise stated. RVs often depend on other random variables. We express that dependency as $X(Y)$. For vectors, $\mathbf{x}(y)$, e.g., $\mathbf{X}(\mathbf{h}) \sim \mathcal{CN}(\mu(\mathbf{h}), \sigma^2)$.

A. Scaling and translation

If $X \sim D$, and $Y = \sigma^2 X + \mu$, with $\sigma^2 > 0$, then the PDF, CDF and MGF can be expressed as:

$$\begin{aligned} f_Y(y) &= \frac{1}{\sigma^2} f_D\left(\frac{y-\mu}{\sigma^2}\right), & F_Y(y) &= F_D\left(\frac{y-\mu}{\sigma^2}\right), \\ M_Y(t) &= e^{\mu t} M_D(\sigma^2 t). \end{aligned} \quad (53)$$

B. Chi-squared (χ^2) Distribution

If $X = \sum_{i=1}^K N_i^2$ with $N_i \sim \mathcal{N}(0, 1)$, then X follows a Chi-squared distribution with K degrees of freedom, $X \sim \chi_{2K}^2$. The PDF, CCDF and MGF are given by:

$$\begin{aligned} f_{\chi_{2\alpha}^2}(x) &= \frac{x^{\alpha-1} e^{-x/2}}{2^\alpha \Gamma(\alpha)}, & \bar{F}_{\chi_{2\alpha}^2}(x) &= \frac{\Gamma(\alpha, \frac{x}{2})}{\Gamma(\alpha)}, \\ M_{\chi_{2\alpha}^2}(t) &= (1 - 2t)^{-\alpha}, & t &< \frac{1}{2}, \end{aligned} \quad (54)$$

with $\Gamma(n, x)$ the upper incomplete gamma function.

C. Non-central χ^2 Distribution (χ'^2)

If $\Psi = \sum_{i=1}^{\alpha} |\ddot{Z}_i|^2$ with $\ddot{Z}_i \sim \mathcal{CN}(\mu_i, 1)$, then Ψ is distributed following a non-central χ^2 distribution with 2α degrees of freedom and $\lambda = \sum_{i=1}^{\alpha} |\mu_i|^2$ as non-centrality parameter. The PDF, CCDF and the MGF of the non-central χ^2 distribution are written as:

$$f_{\chi_{2\alpha}'^2}(x; \lambda) = \frac{1}{2} e^{-\frac{x+\lambda}{2}} \left(\frac{x}{\lambda}\right)^{\frac{\alpha-1}{2}} I_{\alpha-1}(\sqrt{\lambda x}), \quad x > 0 \quad (55)$$

$$\bar{F}_{\chi_{2\alpha}'^2}(x; \lambda) = Q_{\alpha}(\sqrt{\lambda}, \sqrt{x}), \quad x > 0 \quad (56)$$

$$M_{\chi_{2\alpha}'^2}(t; \lambda) = (1 - 2t)^{-\alpha} \exp\left(\frac{\lambda t}{1 - 2t}\right), \quad (57)$$

with $Q_M(a, b)$ the Marcum Q-function of order M .

D. Scaled χ'^2 Distribution

If $\Psi = \sum_{i=1}^{\alpha} |Z_i|^2$ with $Z_i \sim \mathcal{CN}(\mu_i, \sigma^2)$, then Ψ is distributed following a scaled non-central χ^2 distribution with 2α degrees of freedom and $\lambda = \sum_{i=1}^{\alpha} |\mu_i|^2 / \sigma^2$ as non-centrality parameter, that is, $\Psi \sim \sigma^2 \chi_{2\alpha}'^2\left(\sum_{i=1}^{\alpha} |\mu_i|^2 / \sigma^2\right)$. The PDF, CCDF, and MGF of the scaled noncentral χ^2 distribution can be obtained by applying the scale expressions in Subsection IX-A to those in Subsection IX-C.

E. Scaled χ'^2 distribution with scaled χ^2 non-centrality parameter

Let $X \sim \sigma_x^2 \chi_{2\alpha}'^2(\Lambda)$ be a scaled non-central chi-square random variable with 2α DOF and non-centrality parameter Λ . Assume that the non-centrality itself is random, $\Lambda \sim \sigma_\lambda^2 \chi_{2\beta}^2$, where Λ is a scaled central chi-square with 2β DOF. Then, X follows a generalized χ^2 distribution:

$$X \sim \sigma_x^2 \chi_{2(\alpha-\beta)}^2 * \sigma_x^2 (1 + \sigma_\lambda^2) \chi_{2\beta}^2, \quad (58)$$

with $*$ is the convolution operator coming from the addition of two random variables.

Consequently, its CDF is given by:

$$\begin{aligned} F_X(x) &= \\ &= \sum_{j=0}^{\infty} \frac{\Gamma(j+\beta)}{j! \Gamma(\beta)} \left(\frac{\sigma_\lambda^2}{\sigma_\lambda^2 + 1}\right)^j \left(\frac{1}{\sigma_\lambda^2 + 1}\right)^\beta \frac{\gamma\left(\alpha + j, \frac{x}{2\sigma_x^2}\right)}{\Gamma(\alpha + j)}, \end{aligned} \quad (59)$$

where $\gamma(\cdot, \cdot)$ is the lower incomplete gamma function.

In case that $\alpha = \beta$, the result is reduced to an unique scaled χ^2 distribution, $X \sim \sigma_x^2 (1 + \sigma_\lambda^2) \chi_{2\alpha}^2$, with corresponding CDF:

$$F_X(x) = \frac{\gamma\left(\alpha, \frac{x}{2\sigma_x^2(1+\sigma_\lambda^2)}\right)}{\Gamma(\alpha)}. \quad (60)$$

REFERENCES

- [1] 3rd Generation Partnership Project (3GPP), *NR; Physical channels and modulation; (Release 18)*, TS 38.211 V18.2.0, September 2023.
- [2] M. Enescu, *5G New Radio: A beam-based air interface*. John Wiley & Sons, 2020.
- [3] A. Chakrapani, "On the design details of SS/PBCH, signal generation and PRACH in 5G-NR," *IEEE Access*, vol. 8, pp. 136 617–136 637, 2020.
- [4] R.-A. Pitaval, B. M. Popović, P. Wang, and F. Berggren, "Overcoming 5G PRACH capacity shortfall: Supersets of Zadoff–Chu sequences with low-correlation zone," *IEEE Transactions on Communications*, vol. 68, no. 9, pp. 5673–5688, 2020.
- [5] Y. Liang, X. Li, J. Zhang, and Z. Ding, "Non-orthogonal random access for 5G networks," *IEEE Transactions on Wireless Communications*, vol. 16, no. 7, pp. 4817–4831, 2017.
- [6] J. Zhu, Y. Sun, and M. Peng, "Timing advance estimation in low earth orbit satellite networks," *IEEE Transactions on Vehicular Technology*, vol. 73, no. 3, pp. 4366–4382, 2023.
- [7] J. Tao and L. Yang, "Improved Zadoff-Chu sequence detection in the presence of unknown multipath and carrier frequency offset," *IEEE Communications Letters*, vol. 22, no. 5, pp. 922–925, 2018.
- [8] Q. Wang, G. Ren, and J. Wu, "A multiuser detection algorithm for random access procedure with the presence of carrier frequency offsets in LTE systems," *IEEE Transactions on Communications*, vol. 63, no. 9, pp. 3299–3312, 2015.
- [9] X. Yang and A. O. Fapojuwo, "Enhanced preamble detection for PRACH in LTE," in *2013 IEEE Wireless Communications and Networking Conference (WCNC)*. IEEE, 2013, pp. 3306–3311.
- [10] M. Hua, M. Wang, W. Yang, X. You, F. Shu, J. Wang, W. Sheng, and Q. Chen, "Analysis of the frequency offset effect on random access signals," *IEEE Transactions on communications*, vol. 61, no. 11, pp. 4728–4740, 2013.
- [11] J. Ding, D. Qu, and J. Choi, "Analysis of non-orthogonal sequences for grant-free RA with massive MIMO," *IEEE Transactions on Communications*, vol. 68, no. 1, pp. 150–160, 2019.
- [12] T. Kim, I. Bang, and D. K. Sung, "An enhanced PRACH preamble detector for cellular IoT communications," *IEEE Communications Letters*, vol. 21, no. 12, pp. 2678–2681, 2017.
- [13] A. Chakrapani, "NB-IoT uplink receiver design and performance study," *IEEE Internet of Things Journal*, vol. 7, no. 3, pp. 2469–2482, 2019.
- [14] T. Kim, K. S. Ko, and D. K. Sung, "Transmit power optimization for prioritized random access in OFDMA based systems," in *2016 IEEE International Conference on Communications (ICC)*. IEEE, 2016, pp. 1–6.
- [15] Y. Ota, T. Chiba, M. Sawahashi, and S. Suyama, "NR PRACH detection probability in the presence of CFO in multi-access environments," in *2023 VTS Asia Pacific Wireless Communications Symposium (APWCS)*. IEEE, 2023, pp. 1–5.
- [16] 3rd Generation Partnership Project (3GPP), *5G; NR; Physical layer procedures for control*, TS 38.213 v18.6.0, April 2025.
- [17] 3GPP, "5G; NR; Physical channels and modulation," 3rd Generation Partnership Project (3GPP), TS 38.211 v16.07.00, October 2021.
- [18] B. C. Berndt, R. J. Evans, and K. S. Williams, *Gauss and Jacobi sums*. Wiley, 1998.
- [19] 3rd Generation Partnership Project (3GPP), *NR; Base Station (BS) conformance testing; (Release 18)*, TS 38.141-1 V18.10.0, July 2025.
- [20] P. Patnaik, "The non-central χ^2 - and f -distribution and their applications," *Biometrika*, vol. 36, no. 1/2, pp. 202–232, 1949.
- [21] S. Sesia, I. Toufik, and M. Baker, *LTE-the UMTS long term evolution: from theory to practice*. John Wiley & Sons, 2011.